
Stochastic Transition-Map Distillation for Fast Probabilistic Inference

George Rapakoulias¹Peter Garud²Lingjiong Zhu³Panagiotis Tsiotras¹¹ Department of Aerospace Engineering, Georgia Institute of Technology, Atlanta, GA² Department of Computer Science, Georgia Institute of Technology, Atlanta, GA³ Department of Mathematics, Florida State University, Tallahassee, FL

Abstract

Diffusion models achieve strong generation quality, diversity, and distribution coverage, but their performance often comes with expensive inference. In this work, we propose *Stochastic Transition-Map Distillation* (STMD), a teacher-free framework for accelerating diffusion model inference while preserving probabilistic sample generation. In contrast to score-based diffusion models, whose denoising parametrization models the mean of the posterior distribution, STMD distills the full transition map associated with the sampling stochastic differential equation (SDE). We parameterize these SDE transitions with a conditional Mean Flow model, yielding a one- or few-step stochastic sampler that retains the transition structure of the underlying diffusion process. This perspective is especially useful for downstream tasks that require stochastic inference, such as diffusion posterior sampling, inverse problems, and energy-based fine-tuning. Compared to recent distillation methods, STMD requires no pretrained teacher, bi-level optimization, or trajectory simulation and caching, enabling efficient and scalable training. We derive convergence bounds for our method in the Wasserstein distance, providing a strong theoretical foundation for our approach, and validate STMD on various image generation examples on the MNIST, CIFAR-10, and CelebA datasets.

1 Introduction and Motivation

Continuous-time diffusion models excel in generation quality and sample diversity compared to their predecessors, such as Generative Adversarial Networks (GANs) and Variational Autoencoders (VAEs) (Goodfellow et al., 2014, 2020; Arjovsky et al., 2017; Kingma & Welling, 2014, 2019); however, this performance increase comes at the expense of inference complexity, stemming from the need to integrate the underlying continuous-time ordinary differential or stochastic differential equations. Although many techniques have been proposed to accelerate inference, such as distillation (Luhman & Luhman, 2021; Song et al., 2023) and Optimal Transport (OT) based approaches (Liu et al., 2023; Shi et al., 2023), to name a few, achieving the optimal tradeoff between generation quality and sample diversity versus inference complexity is still unresolved (Dieleman, 2024).

Flow Matching (FM) and its variants (Liu et al., 2023; Lipman et al., 2023; Albergo & VandenEijnden, 2023) have emerged as a powerful tool for training continuous-time flow models. They work by approximating the drift term (also referred to as the policy) of an Ordinary Differential Equation (ODE) or Stochastic Differential Equation (SDE) as a mixture of elementary point-to-point conditional drift terms. Implementing Flow Matching in practice, however, requires a temporal

Corresponding authors: grap@gatech.edu, lzhu2@fsu.edu, tsiotras@gatech.edu

discretization of the learned continuous-time ODE/SDE with a very small time step size, slowing down inference (Shi et al., 2023; Lipman et al., 2023).

Distillation techniques offer a set of tools to accelerate inference by learning a flow map of the corresponding ODE directly (Song et al., 2023; Boffi et al., 2025a,b; Geng et al., 2025a,b; Salimans & Ho, 2022). At large, these methods leverage different techniques to “learn to integrate” an underlying continuous-time ODE. Although they achieve high-quality results, one disadvantage is that they are usually used only with deterministic inference, that is, given an initial noise sample, the generated sample is unique. Many downstream tasks, however, benefit from stochastic inference to boost generation quality, improve model alignment with user queries (Holderrieth et al., 2026), or perform diffusion posterior inference based on noisy or partial sample observations (Chung et al., 2023). In this direction, recent works have explored training one- or few-step generators to match the distribution of a diffusion model (Lai et al., 2025, Section 10.2) (Yin et al., 2024; Gushchin et al., 2025; Peng et al., 2025).

In this work, we take a different approach and propose a method for learning the transition probabilities of a given SDE, thereby generalizing ODE-based distillation approaches to the stochastic regime. We achieve this by using a conditional Mean Flow, which learns a single or few-step generator for the transition probability of a diffusion model.

The contributions of this paper are as follows:

- We propose STMD, a distillation framework based on conditional Mean Flows, enabling us to learn the transition maps of high-dimensional diffusion SDEs using a single-step or a few-step generator through a regression objective, and without using any pretrained model.
- We provide a theoretical convergence analysis in the 2-Wasserstein distance for the Mean Flow algorithm, and then extend it to study the convergence of our learned transition map to that of the underlying diffusion process. To the best of our knowledge, this is the first Mean Flow convergence analysis in the 2-Wasserstein distance.
- We illustrate this method in various scenarios related to image generation and inpainting problems, showing strong empirical performance.

2 Preliminaries

2.1 Flow Matching with Straight-Line Interpolants

We first recall the basic Flow Matching formulation (Liu et al., 2023; Lipman et al., 2023; Albergo & Vanden-Eijnden, 2023) with straight-line interpolants. All distributions are supported in the d -dimensional Euclidean space, denoted \mathbb{R}^d . To align with the recently proposed Mean Flow model (Geng et al., 2025a), we will use $z_0 \sim \rho_0$ to denote the data distribution, and $z_1 \sim \rho_1$ to denote a sample from a simple prior distribution, e.g., a Gaussian distribution. We denote the densities of flow-related variables with ρ , and use the variable s to denote time. Unless stated otherwise, all differential equations run backward in time, that is, from $s = 1$ to $s = 0$. For $s \in [0, 1]$, define the straight-line interpolant

$$z_s = (1 - s)z_0 + sz_1. \quad (1)$$

The corresponding conditional velocity is constant along the path and is given by

$$v_s(z_s | z_0, z_1) = z_1 - z_0. \quad (2)$$

A velocity field that transports ρ_0 to ρ_1 and vice versa can be obtained by averaging this conditional velocity over all pairs $(z_0, z_1) \sim \rho_0 \times \rho_1$ that could have produced the same intermediate point z_s :

$$v_s(z) = \mathbb{E}[z_1 - z_0 | z_s = z]. \quad (3)$$

The Flow Matching objective trains a neural network $v_s^\theta(z)$ to approximate (3) using a finite-sample approximation of the conditional flow matching objective (Lipman et al., 2023; Liu et al., 2023):

$$\mathcal{L}_{\text{CFM}} = \mathbb{E} \left[\left\| v_s^\theta(z_s) - (z_1 - z_0) \right\|^2 \right]. \quad (4)$$

This conditional objective is equivalent, in terms of its optimizer, to regression against the marginal velocity $v_s(z)$ defined in (3). Indeed, by expanding (4) and using the tower property of conditional expectation,

$$\mathbb{E} \left[\left\| v_s^\theta(z_s) - (z_1 - z_0) \right\|^2 \right] = \mathbb{E} \left[\left\| v_s^\theta(z_s) - v_s(z_s) \right\|^2 \right] + C, \quad (5)$$

where C is independent of θ , motivating the use of CFM objective (4).

At inference time, samples are generated by integrating the learned ODE backwards from $s = 1$ to $s = 0$:

$$\dot{z}_s = v_s^\theta(z_s). \quad (6)$$

2.2 Consistency Models and Mean Flows

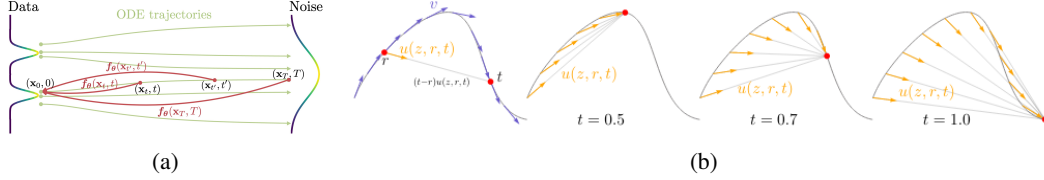


Figure 1: (a): Consistency training learns the flow map of an ODE without requiring sampling of simulated trajectories during training. Figure taken from Song et al. (2023). (b): Mean Flows parametrize the flow map using the average velocity along a trajectory, allowing for taking exact, finite-time steps during inference. Figure taken from Geng et al. (2025a).

A limitation of flow models is that during inference, the learned flow (6) needs to be integrated. To accelerate inference, distillation approaches aim at learning the flow map of the inference ODE:

$$\dot{z}_s = v_s(z_s). \quad (7)$$

Seminal works in this direction include Song et al. (2023); Kim et al. (2024), which are based on the probability flow ODE to model v_s in (7), and Boffi et al. (2025a); Geng et al. (2025a), that leverage a flow-matching ODE and use a drift of the form (3).

A recent work is the Mean Flow (MF) model (Geng et al., 2025a), which learns the flow map of (6) without requiring a pretrained reference model $v_s^\theta(z_s)$. Consider an ODE (7) with drift as in (3). Let $0 \leq r < s \leq 1$. Consider a trajectory starting from z_s at time s , denoted with $\{z_\tau, \tau \in [r, s]\}$. The MF algorithm is based on the concept of average velocity along the flow lines of (6), i.e., the quantity:

$$u(z_s, r, s) = \frac{1}{s - r} \int_r^s v_\tau(z_\tau) d\tau. \quad (8)$$

Since, by definition of a solution of the ODE (6),

$$z_s = z_r - \int_r^s v_\tau(z_\tau) d\tau = z_r - (s - r) u(z_s, r, s), \quad (9)$$

so that a model for $u(z_s, r, s)$ fully describes the flow map of (6). Rearranging and differentiating (8) with respect to time s gives

$$u(z_s, r, s) = v_s(z_s) - (s - r) \frac{d}{ds} u(z_s, r, s), \quad (10)$$

while

$$\frac{d}{ds} u(z_s, r, s) = \frac{\partial u}{\partial z} v_s(z_s) + \frac{\partial u}{\partial s}. \quad (11)$$

The MF model parametrizes the mean velocity in Equation (8) with a neural network, and is trained through the MF objective function, which is a square-norm deviation penalty based on (10):

$$\mathcal{L}_{\text{MF}} = \mathbb{E} \left[\left\| u^\theta(z_s, r, s) - \text{sg} \left(v_s(z_s) - (s - r) \frac{d}{ds} u^\theta(z_s, r, s) \right) \right\|^2 \right]. \quad (12)$$

The sg operator in (12) denotes the stop-gradient operator commonly used in the literature (Song et al., 2023; Song & Dhariwal, 2024; Frans et al., 2025; Geng et al., 2025b; Lu & Song, 2025; Geng et al., 2025a), and is used to stabilize training by avoiding having to backpropagate through the numerical calculation of the Jacobian-vector product related to Equation (11). Since the expression

for $v_s(z_s) = \mathbb{E}[z_1 - z_0 | z_s]$ is not known a priori, similarly with flow matching, the objective (12) is replaced with a tractable conditional objective, and the MF model is trained instead with:

$$\mathcal{L}_{\text{CMF}} = \mathbb{E} \left[\left\| u^\theta(z_s, r, s) - \text{sg} \left((z_1 - z_0) - (s - r) \frac{d}{ds} u^\theta(z_s, r, s) \right) \right\|^2 \right]. \quad (13)$$

The following proposition guarantees the equivalence of minimizing \mathcal{L}_{MF} in (12) and \mathcal{L}_{CMF} in (13). **Proposition 1.** *The loss function \mathcal{L}_{MF} in (12) and the loss function \mathcal{L}_{CMF} given in (13), have the same gradient with respect to the model parameters, that is $\nabla_\theta \mathcal{L}_{\text{CMF}} = \nabla_\theta \mathcal{L}_{\text{MF}}$.*

3 Stochastic Transition-Map Distillation

3.1 Unconditional Diffusion Distillation

Consider a forward diffusion process

$$dx_t = -\frac{1}{2}\beta_t x_t dt + \sqrt{\beta_t} dw_t, \quad x_0 \sim p_0, \quad (14)$$

where w_t is a standard d -dimensional Brownian motion and $\beta_t \geq 0$ is a scalar function of time. To avoid confusion with the Mean Flow variable z_s , we will denote probability densities associated with the diffusion variable x_t using p_t , and denote the diffusion time with t . The SDE (14) is known as the variance-preserving (VP) SDE in the literature (Song et al., 2021). Since (14) is an Ornstein-Uhlenbeck process, the transition density function $p(x_t|x_0)$ of (14) can be parametrized in closed form:

$$x_t = \alpha_t x_0 + \sigma_t \epsilon, \quad \epsilon \sim \mathcal{N}(0, I_d), \quad x_0 \sim p_0, \quad (15)$$

where $\alpha_t^2 := \exp(-\int_0^t \beta_\tau d\tau)$, $\sigma_t := \sqrt{1 - \alpha_t^2}$. Furthermore, the time reversal of (14) is an SDE running backward in time (Anderson, 1982; Föllmer, 1985; Song et al., 2021; Cattiaux et al., 2023):

$$-dx_t = \left[-\frac{1}{2}\beta_t x_t - \beta_t \nabla \log p_t(x_t) \right] dt + \sqrt{\beta_t} dw_t, \quad x_1 \sim p_1, \quad (16)$$

where $\nabla \log p_t(x_t)$ is known as the score function (Schervish, 1995). It is easy to verify that the marginal of (16) matches that of (14) for all time marginals (Anderson, 1982; Song et al., 2021). Score-based diffusion models learn the score function using Tweedie's formula (Efron, 2011):

$$\nabla \log p_t(x_t) = \frac{\alpha_t \mathbb{E}[x_0|x_t] - x_t}{\sigma_t^2}, \quad (17)$$

and by learning the mean of the posterior distribution $p(x_0|x_t)$. Our goal, instead, is to model the weak solution of the SDE (16), that is, given any point x_t along the stochastic trajectories of (16), and some time $t' < t$, predict the corresponding distribution for the state $x_{t'} \sim p(x_{t'}|x_t)$, using a single step generator, without incurring the costly numerical integration of (16). We illustrate this concept in Figure 2.

Instead of modeling $p(x_{t'}|x_t)$ directly, we will use an x_0 -parametrization for our model

$$p(x_{t'}|x_t) = \int_{\mathbb{R}^d} p(x_0|x_t) p(x_{t'}|x_0, x_t) dx_0. \quad (18)$$

Since, for all $0 \leq t' < t \leq 1$, the bridge measure $p(x_{t'}|x_0, x_t)$ is available in closed form for diffusions of the form (14) using Song et al. (2021):

$$p(x_{t'}|x_0, x_t) = \mathcal{N} \left(x_{t'}; \frac{\alpha_{t'}^2 - \alpha_t^2}{\alpha_{t'} \sigma_t^2} x_0 + \frac{\alpha_t \sigma_{t'}^2}{\alpha_{t'} \sigma_t^2} x_t, \frac{\sigma_{t'}^2 (\alpha_{t'}^2 - \alpha_t^2)}{\alpha_{t'}^2 \sigma_t^2} I_d \right), \quad 0 < t' < t, \quad (19)$$

given a parametric model $p^\theta(x_0|x_t)$, sampling from $p(x_{t'}|x_t)$ through (18) is as easy as sampling from $p^\theta(x_0|x_t)$.

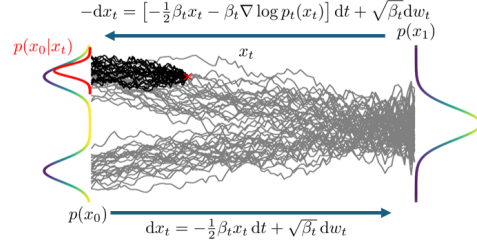


Figure 2: Stochastic Transition-Map Distillation.

We therefore parameterize $p^\theta(x_0|x_t)$ with a conditional Mean Flow, that is, we construct a flow model that maps the prior $z_1 \sim \mathcal{N}(0, I_d)$ to samples from $z_0 \sim p(x_0|x_t)$. Specifically, we define a conditional flow model in the latent variable z_s , conditioned on x_t and t as follows:

$$u(z_s, r, s, x_t, t) = v_s(z_s|x_t, t) - (s-r) \frac{d}{ds} u(z_s, r, s, x_t, t), \quad (20)$$

where $v_s(z_s|x_t, t) = \mathbb{E}[z_1 - x_0|z_s, x_t, t]$. We now define the diffusion MF loss function as

$$\mathcal{L}_{\text{dMF}} = \mathbb{E} \left[\left\| u^\theta(z_s, r, s, x_t, t) - \text{sg} \left(v_s(z_s|x_t, t) - (s-r) \frac{d}{ds} u^\theta(z_s, r, s, x_t, t) \right) \right\|^2 \right]. \quad (21)$$

where the expectation in (21) is taken with respect to x_0, t, x_t, r, s, z_1 . Furthermore, the conditional Mean Flow objective generalizes to

$$\mathcal{L}_{\text{dCMF}} = \mathbb{E} \left[\left\| u^\theta(z_s, r, s, x_t, t) - \text{sg} \left(z_1 - x_0 - (s-r) \frac{d}{ds} u^\theta(z_s, r, s, x_t, t) \right) \right\|^2 \right]. \quad (22)$$

Using a similar argument as in Proposition 1, it is easy to see that the gradients of Equations (21) and (22) with respect to the model parameters θ are the same.

Proposition 2. *The loss function \mathcal{L}_{dMF} in (21) and the loss function $\mathcal{L}_{\text{dCMF}}$ given in (22) have the same gradient with respect to the model parameters, that is, $\nabla_\theta \mathcal{L}_{\text{dCMF}} = \nabla_\theta \mathcal{L}_{\text{dMF}}$.*

To train the model using (22), we only need samples from the joint distribution of $p(x_0, x_t)$. Since sampling from $p(x_0|x_t)$ requires simulations of (16), we use the reverse kernel $p(x_t|x_0)$, which is known in closed form, along with samples from the data distribution $p(x_0)$. We present an overview of the training and sampling algorithms for our conditional Mean Flow model in Algorithm 1 and Algorithm 2, respectively.

Algorithm 1 STMD training

Input: Data distribution samples p_0 , forward SDE scheduler $\{\beta_t, \alpha_t, \sigma_t, t \in [0, 1]\}$, conditional Mean Flow model parametrization $u^\theta(z, r, s, x, t)$.

Sample $x_0 \sim p_0, t \sim \text{unif}(0, 1), x_t$ through (15), $z_1 \sim \mathcal{N}(0, I_d), r, s \sim \text{sample_r_s}()$ ⁰.

$z_s \leftarrow (1-s)x_0 + sz_1$

$u^\theta, \frac{du^\theta}{ds} \leftarrow \text{jvp}(u^\theta, (z_s, r, s, x_t, t), (z_1 - x_0), 0, 1, 0, 0)$

Compute CMF loss $\mathcal{L}_{\text{dCMF}}$ using Equation (22).

Take optimization step on $\mathcal{L}_{\text{dCMF}}$.

return Trained $u^\theta(z_s, r, s, x_t, t)$

Algorithm 2 STMD inference

Input: Trained model $u^\theta(z_s, r, s, x_t, t)$, initial samples $x_1 \sim \mathcal{N}(0, I_d)$, number of inference steps n_{inf} , number of Mean Flow steps n_{mf} .

$\Delta t \leftarrow \frac{1}{n_{\text{inf}}}, \Delta s \leftarrow \frac{1}{n_{\text{mf}}}, t \leftarrow 1,$

for k in $\text{range}(n_{\text{inf}})$ **do:**

$z_1 \sim \mathcal{N}(0, I_d), s \leftarrow 1$

for i in $\text{range}(n_{\text{mf}})$ **do:**

$z_{s-\Delta s} \leftarrow z_s - \Delta s u^\theta(z_s, s - \Delta s, x_t, t)$

$s \leftarrow s - \Delta s$

end for

$x_0 \leftarrow z_0$

$x_{t-\Delta t} \sim p(x_{t-\Delta t}|x_0, x_t)$ from Equation (19)

$t \leftarrow t - \Delta t$

end for

return x_0

⁰We refer the reader to the Appendix D for the detailed sampling strategy for r, s .

3.2 Convergence Theory

In this section, we obtain Wasserstein convergence guarantees for the Mean Flow model, and then generalize them to show that our conditional Mean Flow model converges to the transition kernel of the reverse SDE (16). To the best of our knowledge, this is the first result showing convergence of the Mean Flow algorithm in the Wasserstein distance.

Let $\mathcal{P}_2(\mathbb{R}^d)$ be the space of all Borel probability measures on \mathbb{R}^d with finite second moment (with respect to the Euclidean norm). For any two Borel probability measures μ, ν in $\mathcal{P}_2(\mathbb{R}^d)$, the 2-Wasserstein distance between μ and ν is defined as (Villani, 2008): $\mathcal{W}_2^2(\mu, \nu) := \inf_{\gamma \in \Pi(\mu, \nu)} \int_{\mathbb{R}^d \times \mathbb{R}^d} \|x - y\|^2 d\gamma(x, y)$, where $\Pi(\mu, \nu)$ is the set of couplings of (μ, ν) .

We will first study the convergence of the unconditional Mean Flow model, presented in Section 2.2. Recall that sampling using the Mean Flow model can be achieved via:

$$z_r = z_s - (s - r)u(z_s, r, s). \quad (23)$$

In the case of single-step sampling, we have $z_0 = z_1 - u(z_1, 0, 1)$ with $z_1 \sim \rho_1$. Next, we obtain the Wasserstein convergence guarantees for the Mean Flow model for the single-step generator $\hat{z}_0 = z_1 - \hat{u}(z_1, 0, 1)$ with $z_1 \sim \rho_1$, where \hat{u} is a candidate mean velocity field. First, given the candidate model \hat{u} , and for fixed r, s we define the (r, s) -conditional Mean Flow error, as

$$\varepsilon_{r,s} := \mathbb{E}_{z_s} \left[\left\| \hat{u}(z_s, r, s) - \text{sg} \left(v_s(z_s) - (s - r) \frac{d}{ds} \hat{u}(z_s, r, s) \right) \right\|^2 \right]. \quad (24)$$

Note the Mean Flow loss reduces to $\mathcal{L}_{\text{MF}} = \mathbb{E}_{r,s}[\varepsilon_{r,s}]$. We now state our main convergence theorem. **Theorem 1.** *Let $\hat{\rho}_0$ denote the single-step generated distribution of $\hat{z}_0 = z_1 - \hat{u}(z_1, 0, 1)$ with $z_1 \sim \rho_1$, where \hat{u} is a candidate mean velocity field. Assume that $\mathbb{E}_s[\varepsilon_{0,s}] \leq \varepsilon$. Then,*

$$\mathcal{W}_2^2(\hat{\rho}_0, \rho_0) \leq e\varepsilon. \quad (25)$$

Notice that the assumption that $\mathbb{E}_s[\varepsilon_{0,s}]$ is small is reasonable when training with the loss $\mathcal{L}_{\text{MF}} = \mathbb{E}_{r,s}[\varepsilon_{r,s}]$, since we are minimizing this loss for all values of $r < s$. It is also a standard assumption in the literature Boffi et al. (2025b). Theorem 1 provides the theoretical convergence guarantees in the 2-Wasserstein distance for the Mean Flow model introduced in Geng et al. (2025a), which bridges a gap between theory and practice.

We now study the convergence of the conditional Mean Flow model (20) to the SDE transition kernel $p(x_0|x_t)$ associated with (16). Let $\hat{p}_{0|t}(x_0|x_t)$ be the single-step generated distribution of $\hat{z}_0 = z_1 - \hat{u}(z_1, 0, 1, x_t, t)$, where $z_1 \sim \rho_1$ and \hat{u} is a candidate conditional Mean Flow model. Furthermore, given $\hat{u} = \hat{u}(z_s, r, s, x_t, t)$, define the (t, x_t) -conditional mean flow error as

$$\gamma(r, s, t, x_t) := \mathbb{E}_{z_s} \left[\left\| \hat{u} - \left(v_s(z_s|x_t, t) - (s - r) \frac{d}{ds} \hat{u} \right) \right\|^2 \right]. \quad (26)$$

Given (26), the conditional Mean Flow loss (21) equals $\mathcal{L}_{\text{dMF}} = \mathbb{E}_{r,s,t,x_t}[\gamma(r, s, t, x_t)]$. The following is a corollary of Theorem 1.

Corollary 1. *For a given t, x_t , let $\hat{p}_{0|t}(x_0|x_t)$ denote the single-step generated distribution of $\hat{z}_0 = z_1 - \hat{u}(z_1, 0, 1, x_t, t)$ with $z_1 \sim \rho_1$, where \hat{u} is a candidate conditional mean velocity field. Assume that $\mathbb{E}_{s,t,x_t}[\gamma(0, s, t, x_t)] \leq \varepsilon$. Then,*

$$\mathbb{E}_{t,x_t} [\mathcal{W}_2^2(\hat{p}(x_0|x_t), p(x_0|x_t))] \leq e\varepsilon. \quad (27)$$

Note that during the inference of the diffusion model using (16), we use $x_1 \sim \mathcal{N}(0, I_d)$ where $\mathcal{N}(0, I_d)$ is a proxy of the density $x_1 \sim p_1$ given from (14). This introduces an additional source of error in the generated distribution for x_0 in our conditional Mean Flow model. In the following proposition, we account for this error.

Proposition 3. *Let $\hat{p}(x_0|x_t)$ be a candidate conditional Mean Flow model that parametrizes the transition dynamics of the reverse SDE kernel (16), and let $\tilde{p}_0 = \int_{\mathbb{R}^d} \hat{p}(x_0|x_1) \mathcal{N}(x_1; 0, I_d) dx_1$ and $\hat{\rho}_0 = \int_{\mathbb{R}^d} \hat{p}(x_0|x_1) p(x_1) dx_1$ where $p_1(x_1)$ is the density of x_1 associated with (16). Assuming that $m_2 = \mathbb{E}[\|x_0\|^2] < \infty$, we obtain*

$$\mathcal{W}_2^2(\hat{p}_0, \tilde{p}_0) \leq L^2 (\alpha_1^2 m_2 + (1 - \sigma_1)^2 d), \quad (28)$$

where α_1, σ_1 are defined through (15) and d denotes the problem dimension, provided that the map $\hat{u}(z_1, 0, 1, x_1, 1)$ is L -Lipschitz in x_1 in expectation over z_1 , that is, for any x_1, x'_1 ,

$$\mathbb{E}_{z_1} [\|\hat{u}(z_1, 0, 1, x_1, 1) - \hat{u}(z_1, 0, 1, x'_1, 1)\|^2] \leq L^2 \|x_1 - x'_1\|^2. \quad (29)$$

In Proposition 3, a sufficient condition for (29) is that \hat{u} be uniformly L -Lipschitz in x_1 for all z_1 ; however assuming (45) directly is a weaker condition. The Lipschitz condition is common in the literature; for example, it is often assumed that the candidate velocity field \hat{v}_t is Lipschitz in space uniformly in t in flow models (Albergo & Vanden-Eijnden, 2023; Boffi et al., 2025a). Moreover, the finiteness of the second moment assumption on the data distribution, i.e. $m_2 = \mathbb{E}\|x_0\|^2 < \infty$, is also very mild and commonly assumed in the literature of diffusion models (Chen et al., 2023a,b). Moreover, we will show that if we assume that \tilde{p}_1 and \hat{p}_1 have bounded support, which is a common assumption in the setting when the data distribution p_0 has bounded support, then we can remove the Lipschitz assumption (29); see Proposition 4 in Appendix B for details.

Finally, by applying Corollary 1 and Proposition 3, we obtain the following corollary that provides an upper bound on the 2-Wasserstein distance between the distribution of the output of the conditional Mean Flow model and the true data distribution.

Corollary 2. *Under the assumptions of Theorem 1, Corollary 1, and Proposition 3, we have*

$$\mathcal{W}_2^2(\tilde{p}_0, p_0) \leq 2 \left(L^2 (\alpha_1^2 m_2 + (1 - \sigma_1)^2 d) + e\varepsilon_1 \right), \quad (30)$$

provided that $\mathbb{E}_{s, x_1} [\gamma(0, s, 1, x_1)] \leq \varepsilon_1$, where α_1, σ_1 are defined through (15).

Note that in Corollary 2, the term $\alpha_1^2 m_2 + (1 - \sigma_1)^2 d$ and hence the right hand side in (30) can be made arbitrarily small by taking α_1 to be small (so that $\sigma_1 = \sqrt{1 - \alpha_1^2}$ is close to 1); see Corollary 5 in Appendix B for details.

4 Related Literature

Fast deterministic inference and flow-map distillation. A large body of work accelerates inference of flow-based models by replacing the expensive numerical integration of the learned flow with learned finite-time maps. An early work in this direction is Luhman & Luhman (2021), succeeded by Progressive distillation (Salimans & Ho, 2022), consistency models (Song et al., 2023), consistency trajectory models (Kim et al., 2024), flow maps (Boffi et al., 2025a) and Mean Flows (Geng et al., 2025a), among others. They all aim to reduce the number of function evaluations required at inference time, and can be broadly viewed as learning to integrate an underlying ODE of the flow model. However, they are primarily designed for deterministic generation, usually through the probability-flow ODE or a deterministic flow model. In contrast, our goal is not only to compress the inference trajectory, but also to preserve the stochastic transition structure of the reverse SDE. STMD therefore learns a conditional stochastic transition map, rather than a deterministic noise-to-data map.

Probabilistic denoising and distributional distillation. Several works have recognized that coarse reverse-time stochastic sampling requires more than the conditional mean predicted by standard denoising diffusion models. Denoising Diffusion GANs (Xiao et al., 2022) and Adversarial Schrödinger Bridge Matching (Gushchin et al., 2024) model large transitions with a multimodal conditional GAN, enabling fewer denoising steps by replacing the Gaussian small-step discretization of the inference SDE with a learned stochastic transition. Distributional Diffusion Models with Scoring Rules (De Bortoli et al., 2025) similarly learn a stochastic denoiser for the full posterior distribution $p(x_0|x_t)$, using proper scoring rules such as energy distance or maximum mean discrepancy. NCVSD (Peng et al., 2025) also trains a noise-conditional stochastic denoiser, but does so by distilling a pretrained diffusion teacher through a variational score-distillation objective. These works are closest to STMD in target objective, as they also aim to model the distribution of the denoising posterior. The main distinction is the training principle: DDGAN relies on adversarial training, Distributional Diffusion Models rely on scoring-rule losses, and NCVSD relies on teacher-based score distillation. STMD instead uses a teacher-free, regression-based conditional Mean Flow objective to learn the finite-time transition kernel associated with the reverse SDE.

Distribution matching and bridge distillation. A related family of methods distill diffusion or bridge models by matching generated distributions rather than explicitly matching transition kernels. Distribution Matching Distillation Yin et al. (2024) trains a one-step generator by minimizing a KL-based objective between the generated distribution and the distribution induced by a pretrained

diffusion model. Inverse Bridge Matching Distillation (Gushchin et al., 2025) extends this idea to bridge-matching models by learning a stochastic generator whose induced bridge model matches a pretrained bridge vector field. These methods are effective for fast generation, but they primarily match endpoint marginals, rather than learning the conditional transition kernel $p(x_{t'}|x_t)$ of the sampling SDE. Furthermore, unlike our approach, they require a pretrained diffusion or bridge matching model during training.

Transition matching and discrete stochastic generators. Focusing on discrete-time inference, recent transition-matching methods also emphasize learning expressive stochastic transitions between intermediate generative states, and have been proposed as flexible alternatives to diffusion and flow matching for efficient and probabilistic generation (Shaul et al., 2025). Transition Matching Distillation (Nie et al., 2026) further applies this idea to few-step generation by distilling long diffusion trajectories into a compact transition process. These methods share the goal of accelerating inference through learned transitions with STMD, and also share the concept of using a flow model to model coarse transitions. However, their acceleration principle lies in a patch-based modeling of the transition flow, while the stochasticity of the generator is associated with a bridge model, rather than a diffusion process. STMD instead uses full-state flow model to parametrize transition, and its acceleration is based on distillation.

5 Experiments

We conduct a series of experiments to validate our approach for various image generation and conditional sampling tasks. All our models are trained on a single RTX 5090 GPU. To allow for fair comparisons when comparing with baselines, we use the same neural network backbone for all approaches and train from scratch for the same number of iterations. Although the small number of iterations used in all experiments prevents our networks from achieving state-of-the-art performance, our experiments allow for a comparative study against baselines.

MNIST Example. We first test our method on the MNIST dataset (LeCun et al., 2010). We parametrize the Mean Flow model with a U-Net (Ronneberger et al., 2015) using the diffusers toolbox (von Platen et al., 2022) and PyTorch (Paszke et al., 2019). We provide the exact hyperparameters of the network in Appendix D. We concatenate the flow variable z_s and the diffusion conditioning x_t along the channel axis and use sinusoidal conditioning and a multilayer ResNet for mixing the conditioning variables r, s, t . Following Geng et al. (2025a), instead of feeding all three time steps directly into the conditional Mean Flow network, we found that the model performs best when using $s - r, s, t$ conditioning instead of r, s, t (see inference Algorithm 2). We illustrate generated samples using STMD with different numbers of inference steps n_{mf}, n_{inf} in Figure 3a.

To benchmark our model, since the Fréchet inception distance (FID) scores (Heusel et al., 2017) can be unreliable in the MNIST dataset (Song & Ermon, 2019), as common in the literature, we report Fréchet distance (FD) calculated in the latent space of a MNIST classifier in Figure 3b. We defer the details of the classifier used to Appendix D. Using our FD metric, we compare our model against the original Mean Flow algorithm (Geng et al., 2025a) and a Denoising Diffusion Probabilistic Model (DDPM) baseline (Ho et al., 2020), while ablating the number of inference steps for each method. We present the results in Figure 3b, where we denote the total number of function evaluations (NFE) during the inference loop of each method on the horizontal axis and the FD score on the vertical axis. We use the same network, trained for the same number of iterations, for all three methods. For the FD calculation, we use 10K generated samples and 10K samples from the test dataset.

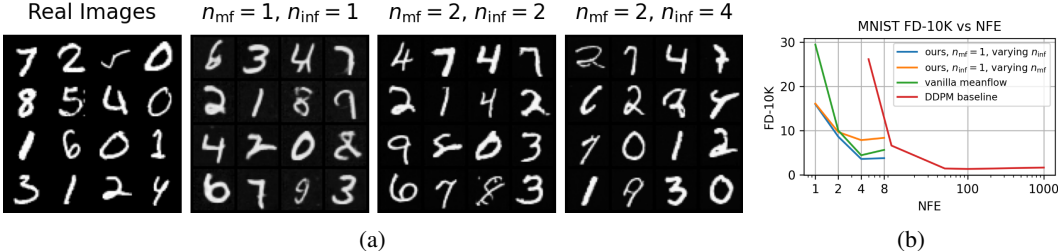


Figure 3: (a): Unconditional MNIST samples using various n_{inf}, n_{mf} (b): MNIST FD vs NFE.



Figure 4: (a): Unconditional CIFAR10 samples using various n_{inf}, n_{mf} (b): CIFAR10 FID vs NFE.

CIFAR10. Next, we test our model in unconditional generation on the CIFAR10 dataset (Krizhevsky & Hinton, 2009). We provide data generated with our STMD approach for a varying number of NFEs in Figure 4a. Similarly to our MNIST experiment, we used 10K samples from the test set of the dataset to compute FID scores and facilitate computations using the `torchmetrics` toolkit (Detlefsen et al., 2022). As in the previous example, we compare our model with a DDPM and an original Mean Flow baseline, using the same network and the same number of training iterations for all experiments. We defer the descriptions of these parameters to Appendix D. We observe that for a fixed number of training iterations, our model performs comparatively with the mean flow model, while retaining full stochasticity of the diffusion-based sampler.

CelebA. Finally, we conduct experiments using the CelebA (Liu et al., 2015) dataset using a latent DiT architecture (Peebles & Xie, 2023). Specifically, we use a DiT/M2 network from Geng et al. (2025a) using an additional temporal conditioning signal for the diffusion time t . We showcase unconditional samples generated with our model in Figure 5 and an inpainting example in Figure 6. We defer the details of the inpainting algorithm to the Appendix C. For the unconditional image generation, we used $n_{inf} = 4$ and $n_{mf} = 2$ and calculated an FID score of 8.28, using 10K samples from the test dataset. For inpainting, we use $n_{mf} = 2$, and a total of 50 inference steps.

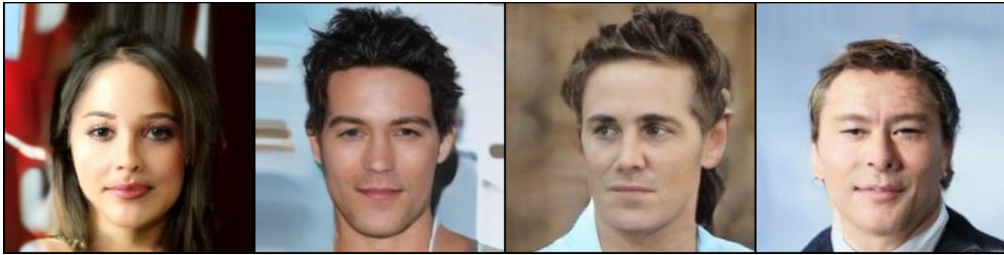


Figure 5: Unconditional generation on the CelebA dataset.



Figure 6: Image inpainting on the CelebA dataset. From left to right: original image, masked image, inpainted image.

6 Conclusions and Limitations

To conclude, we introduce STMD, a framework for distilling the transition maps of diffusion models into one- or few-step generators. Unlike state-of-the-art methods for the same task, our model

does not require a pretrained teacher model or bilevel optimization algorithms during training. We establish a strong theoretical foundation for our approach and derive a convergence result for the Mean Flow model in the Wasserstein distance. We then generalize this result to our STMD model and show that it converges in expectation to the transition kernel of the inference process of the reference sampling diffusion and that the generated sample distribution converges to that of the data. Finally, we demonstrate our method on a comprehensive set of image generation and inpainting experiments over the MNIST, CIFAR10, and CelebA datasets and show that our method performs in line with baselines, while allowing for probabilistic sampling and requiring only a small number of inference steps.

References

- Albergo, M. and Vanden-Eijnden, E. Building normalizing flows with stochastic interpolants. In *International Conference on Learning Representations*, Kigali Rwanda, May 2023.
- Anderson, B. D. O. Reverse-time diffusion equation models. *Stochastic Processes and their Applications*, 12(3):313–326, 1982.
- Arjovsky, M., Chintala, S., and Bottou, L. Wasserstein generative adversarial networks. In *International Conference on Machine Learning*, volume 70, pp. 214–223, Sydney, Australia, 2017. PMLR.
- Bakry, D., Gentil, I., and Ledoux, M. *Analysis and Geometry of Markov Diffusion Operators*, volume 348. Springer, Cham, 2014.
- Boffi, N., Albergo, M., and Vanden-Eijnden, E. How to build a consistency model: Learning flow maps via self-distillation. In Belgrave, D., Zhang, C., Lin, H., Montoya, L., Pascanu, R., Koniusz, P., Ghassemi, M., and Chen, N. (eds.), *Advances in Neural Information Processing Systems*, volume 38, pp. 33346–33382. Curran Associates, Inc., 2025a.
- Boffi, N. M., Albergo, M. S., and Vanden-Eijnden, E. Flow map matching with stochastic interpolants: A mathematical framework for consistency models. *Transactions on Machine Learning Research*, 05:1–28, 2025b.
- Cattiaux, P., Conforti, G., Gentil, I., and Léonard, C. Time reversal of diffusion processes under a finite entropy condition. *Annales de l’Institut Henri Poincaré, Probabilités et Statistiques*, 59(4): 1844–1881, 2023.
- Chen, H., Lee, H., and Lu, J. Improved analysis of score-based generative modeling: User-friendly bounds under minimal smoothness assumptions. In *International Conference on Machine Learning*, volume 202, pp. 4764–4803. PMLR, 2023a.
- Chen, S., Chewi, S., Li, J., Li, Y., Salim, A., and Zhang, A. R. Sampling is as easy as learning the score: Theory for diffusion models with minimal data assumptions. In *International Conference on Learning Representations*, 2023b.
- Chung, H., Kim, J., Mccann, M. T., Klasky, M. L., and Ye, J. C. Diffusion posterior sampling for general noisy inverse problems. In *International Conference on Learning Representations*, 2023.
- De Bortoli, V., Galashov, A., Guntupalli, J. S., Zhou, G., Murphy, K., Gretton, A., and Doucet, A. Distributional diffusion models with scoring rules. In *Proceedings of the 42nd International Conference on Machine Learning*, volume 267, pp. 12632–12676. PMLR, 2025.
- Detlefsen, N. S., Borovec, J., Schock, J., Harsh, A., Koker, T., Di Liello, L., Stancl, D., Quan, C., Grechkin, M., and Falcon, W. TorchMetrics: Measuring reproducibility in PyTorch. *Journal of Open Source Software*, 2022. URL <https://github.com/Lightning-AI/torchmetrics>.
- Dieleman, S. The paradox of diffusion distillation, 2024. URL <https://sander.ai/2024/02/28/paradox.html>.
- Efron, B. Tweedie’s formula and selection bias. *Journal of the American Statistical Association*, 106: 1602–1614, 2011.

- Föllmer, H. An entropy approach to the time reversal of diffusion processes. In Metivier, M. and Pardoux, E. (eds.), *Stochastic Differential Systems Filtering and Control*, pp. 156–163, Berlin, Heidelberg, 1985. Springer.
- Frans, K., Hafner, D., Levine, S., and Abbeel, P. One step diffusion via shortcut models. In *International Conference on Learning Representations*, 2025.
- Geng, Z., Deng, M., Bai, X., Kolter, Z., and He, K. Mean flows for one-step generative modeling. In Belgrave, D., Zhang, C., Lin, H., Montoya, L., Pascanu, R., Koniusz, P., Ghassemi, M., and Chen, N. (eds.), *Advances in Neural Information Processing Systems*, volume 38, pp. 75460–75482. Curran Associates, Inc., 2025a.
- Geng, Z., Pokle, A., Luo, W., Lin, J., and Kolter, J. Z. Consistency models made easy. In *International Conference on Learning Representations*, 2025b.
- Gibbs, A. L. and Su, F. E. On choosing and bounding probability metrics. *International Statistical Review*, 70(3):419–435, 2002.
- Goodfellow, I., Pouget-Abadie, J., Mirza, M., Xu, B., Warde-Farley, D., Ozair, S., Courville, A., and Bengio, Y. Generative adversarial nets. In *Advances in Neural Information Processing Systems*, volume 27. Curran Associates, Inc., 2014.
- Goodfellow, I., Pouget-Abadie, J., Mirza, M., Xu, B., Warde-Farley, D., Ozair, S., Courville, A., and Bengio, Y. Generative adversarial networks. *Communications of the ACM*, 63(11):139–144, 2020.
- Graikos, A., Jojic, N., and Samaras, D. Fast constrained sampling in pre-trained diffusion models. In Belgrave, D., Zhang, C., Lin, H., Pascanu, R., Koniusz, P., Ghassemi, M., and Chen, N. (eds.), *Advances in Neural Information Processing Systems*, volume 38, pp. 48205–48240. Curran Associates, Inc., 2025.
- Gushchin, N., Selikhanovych, D., Kholkin, S., Burnaev, E., and Korotin, A. Adversarial Schrödinger bridge matching. In *Advances in Neural Information Processing Systems*, volume 37, pp. 89612–89651. Curran Associates, Inc., 2024.
- Gushchin, N., Li, D., Selikhanovych, D., Burnaev, E., Baranchuk, D., and Korotin, A. Inverse bridge matching distillation. In *Forty-second International Conference on Machine Learning*, volume 267, pp. 21471–21496. PMLR, 2025.
- Heusel, M., Ramsauer, H., Unterthiner, T., Nessler, B., and Hochreiter, S. GANs trained by a two time-scale update rule converge to a local Nash equilibrium. In *Advances in Neural Information Processing Systems*, volume 30. Curran Associates, Inc., 2017.
- Ho, J., Jain, A., and Abbeel, P. Denoising diffusion probabilistic models. In *Advances in Neural Information Processing Systems*, volume 33, pp. 6840–6851. Curran Associates, Inc., 2020.
- Holderrieth, P., Chen, D., Eyring, L., Shah, I., Anantharaman, G., He, Y., Akata, Z., Jaakkola, T., Boffi, N. M., and Simchowitz, M. Diamond maps: Efficient reward alignment via stochastic flow maps, February 2026. URL <http://arxiv.org/abs/2602.05993>. arXiv:2602.05993 [cs].
- Kim, D., Lai, C.-H., Liao, W.-H., Murata, N., Takida, Y., Uesaka, T., He, Y., Mitsufuji, Y., and Ermon, S. Consistency trajectory models: Learning probability flow ODE trajectory of diffusion. In *International Conference on Learning Representations*, 2024.
- Kingma, D. P. and Welling, M. Auto-encoding variational Bayes. In *International Conference on Learning Representations*, 2014.
- Kingma, D. P. and Welling, M. An introduction to variational autoencoders. *Foundations and Trends® in Machine Learning*, 12(4):307–392, 2019.
- Krizhevsky, A. and Hinton, G. Learning multiple layers of features from tiny images. Technical report, University of Toronto, Toronto, Ontario, 2009. URL <https://www.cs.toronto.edu/~kriz/learning-features-2009-TR.pdf>.

- Lai, C.-H., Song, Y., Kim, D., Mitsufuji, Y., and Ermon, S. The principles of diffusion models. *arXiv preprint arXiv:2510.21890*, 2025.
- LeCun, Y., Cortes, C., and Burges, C. MNIST handwritten digit database. *ATT Labs [Online]*. Available: <http://yann.lecun.com/exdb/mnist>, 2, 2010.
- Lipman, Y., Chen, R. T. Q., Ben-Hamu, H., Nickel, M., and Le, M. Flow matching for generative modeling. In *International Conference on Learning Representations*, Kigali Rwanda, May 2023.
- Liu, X., Gong, C., and Liu, Q. Flow straight and fast: Learning to generate and transfer data with rectified flow. In *International Conference on Learning Representations*, Kigali Rwanda, May 2023.
- Liu, Z., Luo, P., Wang, X., and Tang, X. Deep learning face attributes in the wild. In *Proceedings of the IEEE International Conference on Computer Vision*, pp. 3730–3738, 2015.
- Lu, C. and Song, Y. Simplifying, stabilizing and scaling continuous-time consistency models. In *International Conference on Learning Representations*, 2025.
- Luhman, E. and Luhman, T. Knowledge distillation in iterative generative models for improved sampling speed. *arXiv preprint arXiv:2101.02388*, 2021.
- Nie, W., Berner, J., Ma, N., Liu, C., Xie, S., and Vahdat, A. Transition matching distillation for fast video generation. *arXiv preprint arXiv:2601.09881*, 2026.
- Paszke, A., Gross, S., Massa, F., Lerer, A., Bradbury, J., Chanan, G., Killeen, T., Lin, Z., Gimelshein, N., Antiga, L., Desmaison, A., Köpf, A., Yang, E., DeVito, Z., Raison, M., Tejani, A., Chilamkurthy, S., Steiner, B., Fang, L., Bai, J., and Chintala, S. PyTorch: An imperative style, high-performance deep learning library. In *Advances in Neural Information Processing Systems*, volume 32, pp. 8026 – 8037, Vancouver, Canada, 2019. Curran Associates, Inc.
- Peebles, W. and Xie, S. Scalable Diffusion Models with Transformers. In *2023 IEEE/CVF International Conference on Computer Vision (ICCV)*, pp. 4172–4182, Paris, France, October 2023. IEEE.
- Peng, X., Zheng, Z., Wang, Y., Li, H., Kan, N., Dai, W., Li, C., Zou, J., and Xiong, H. Noise conditional variational score distillation. In *Proceedings of the 42nd International Conference on Machine Learning*, volume 267, pp. 48923–48947. PMLR, 2025.
- Ronneberger, O., Fischer, P., and Brox, T. U-net: Convolutional networks for biomedical image segmentation. In *International Conference on Medical Image Computing and Computer-Assisted Intervention*, pp. 234–241. Springer, 2015.
- Salimans, T. and Ho, J. Progressive distillation for fast sampling of diffusion models. In *International Conference on Learning Representations*, 2022.
- Schervish, M. J. *Theory of Statistics*. Springer, 1995.
- Shaul, N., Singer, U., Gat, I., and Lipman, Y. Transition matching: Scalable and flexible generative modeling. In Belgrave, D., Zhang, C., Lin, H., Pascanu, R., Koniusz, P., Ghassemi, M., and Chen, N. (eds.), *Advances in Neural Information Processing Systems*, volume 38, pp. 124347–124388. Curran Associates, Inc., 2025.
- Shi, Y., De Bortoli, V., Campbell, A., and Doucet, A. Diffusion Schrödinger bridge matching. In *Advances in Neural Information Processing Systems*, volume 36, pp. 62183–62223. Curran Associates, Inc., 2023.
- Song, Y. and Dhariwal, P. Improved techniques for training consistency models. In *International Conference on Learning Representations*, 2024.
- Song, Y. and Ermon, S. Generative modeling by estimating gradients of the data distribution. In Wallach, H., Larochelle, H., Beygelzimer, A., d'Alché-Buc, F., Fox, E., and Garnett, R. (eds.), *Advances in Neural Information Processing Systems*, volume 32. Curran Associates, Inc., 2019.

- Song, Y., Sohl-Dickstein, J., Kingma, D. P., Kumar, A., Ermon, S., and Poole, B. Score-based generative modeling through stochastic differential equations. In *International Conference on Learning Representations*, held virtually, 2021.
- Song, Y., Dhariwal, P., Chen, M., and Sutskever, I. Consistency models. In *Proceedings of the 40th International Conference on Machine Learning*, volume 202, pp. 32211–32252. PMLR, 2023.
- Villani, C. *Optimal Transport: Old and New*, volume 338. Springer, 2008.
- von Platen, P., Patil, S., Lozhkov, A., Cuenca, P., Lambert, N., Rasul, K., Davaadorj, M., Nair, D., Paul, S., Berman, W., Xu, Y., Liu, S., and Wolf, T. Diffusers: State-of-the-art diffusion models. <https://github.com/huggingface/diffusers>, 2022.
- Wang, Y., Yu, J., and Zhang, J. Zero-shot image restoration using denoising diffusion null-space model. In *International Conference on Learning Representations*, 2023.
- Xiao, Z., Kreis, K., and Vahdat, A. Tackling the Generative Learning Trilemma with Denoising Diffusion GANs. In *International Conference on Learning Representations*, 2022.
- Yin, T., Gharbi, M., Zhang, R., Shechtman, E., Durand, F., Freeman, W. T., and Park, T. One-step diffusion with distribution matching distillation. In *Proceedings of the IEEE/CVF Conference on Computer Vision and Pattern Recognition*, pp. 6613–6623, 2024.

Stochastic Transition-Map Distillation for Fast Probabilistic Inference

Supplementary Material

The supplementary material is organized as follows.

- In Appendix A, we provide the technical proofs of the main results in the paper.
- In Appendix B, we present additional technical results and their proofs.
- In Appendix C, we discuss inverse problems using STMD.
- In Appendix D, we provide additional details about our numerical experiments.

A Proofs of the Main Results

A.1 Proof of Proposition 1

Proof. Let $v_s(z_s) = \mathbb{E}[z_1 - z_0 | z_s]$. Starting with Equation (13), we obtain

$$\begin{aligned}
\mathcal{L}_{\text{CMF}} &= \mathbb{E} \left[\left\| u^\theta(z_s, r, s) - \text{sg} \left((z_1 - z_0) - v_s(z_s) + v_s(z_s) - (s - r) \frac{d}{ds} u^\theta(z_s, r, s) \right) \right\|^2 \right] \\
&= \mathbb{E} \left[\left\| u^\theta(z_s, r, s) - \text{sg} \left(v_s(z_s) - (s - r) \frac{d}{ds} u^\theta(z_s, r, s) \right) \right\|^2 \right] \\
&\quad + \mathbb{E} \left[\|(z_1 - z_0) - v_s(z_s)\|^2 \right] \\
&\quad + 2\mathbb{E} \left[\left\langle u^\theta(z_s, r, s) - \text{sg} \left(v_s(z_s) - (s - r) \frac{d}{ds} u^\theta(z_s, r, s) \right), (z_1 - z_0) - v_s(z_s) \right\rangle \right] \\
&= \mathcal{L}_{\text{MF}} + \mathbb{E} \left[\|(z_1 - z_0) - v_s(z_s)\|^2 \right].
\end{aligned}$$

By taking the gradient on both sides, and observing that the second term in the final equation does not depend on the model parameters, we obtain $\nabla_\theta \mathcal{L}_{\text{CMF}} = \nabla_\theta \mathcal{L}_{\text{MF}}$, which concludes the proof. \square

A.2 Proof of Proposition 2

Proof. The proof follows the similar steps as in the proof of Proposition 1. Let $v_s(z_s|x_t, t) = \mathbb{E}[z_1 - x_0|z_s, x_t, t]$. Starting with Equation (22), we obtain

$$\begin{aligned}
\mathcal{L}_{\text{dCMF}} &= \mathbb{E} \left[\left\| u^\theta(z_s, r, s, x_t, t) \right. \right. \\
&\quad \left. \left. - \text{sg} \left((z_1 - x_0) - v_s(z_s|x_t, t) + v_s(z_s|x_t, t) - (s-r) \frac{d}{ds} u^\theta(z_s, r, s, x_t, t) \right) \right\|^2 \right] \\
&= \mathbb{E} \left[\left\| u^\theta(z_s, r, s, x_t, t) - \text{sg} \left(v_s(z_s|x_t, t) - (s-r) \frac{d}{ds} u^\theta(z_s, r, s, x_t, t) \right) \right\|^2 \right] \\
&\quad + \mathbb{E} \left[\|(z_1 - x_0) - v_s(z_s|x_t, t)\|^2 \right] \\
&\quad + 2\mathbb{E} \left[\left\langle u^\theta(z_s, r, s) - \text{sg} \left(v_s(z_s|x_t, t) - (s-r) \frac{d}{ds} u^\theta(z_s, r, s) \right), \right. \right. \\
&\quad \quad \quad \left. \left. (z_1 - x_0) - v_s(z_s|x_t, t) \right\rangle \right] \\
&= \mathcal{L}_{\text{dMF}} + \mathbb{E} \left[\|(z_1 - x_0) - v_s(z_s|x_t, t)\|^2 \right].
\end{aligned}$$

By taking the gradient on both sides, and observing that the second term in the final equation does not depend on the model parameters, we obtain $\nabla_\theta \mathcal{L}_{\text{dCMF}} = \nabla_\theta \mathcal{L}_{\text{dMF}}$, which concludes the proof. \square

A.3 Proof of Theorem 1

Proof. Let $z_0 = z_1 - u(z_1, 0, 1)$ and $\hat{z}_0 = z_1 - \hat{u}(z_1, 0, 1)$ where $z_1 \sim \rho_1$. Then $z_0 \sim \rho_0$ and $\hat{z}_0 \sim \hat{\rho}_0$.

By the definition of the 2-Wasserstein distance, we have the bound:

$$\mathcal{W}_2^2(\hat{\rho}_0, \rho_0) \leq \mathbb{E} \|u(z_1, 0, 1) - \hat{u}(z_1, 0, 1)\|^2. \quad (31)$$

To upper bound the right-hand side of (31), let us introduce:

$$E_{r,s} := \mathbb{E}_{z_s} \|(z_s - (s-r)u(z_s, r, s)) - (z_s - (s-r)\hat{u}(z_s, r, s))\|^2, \quad (32)$$

for any $0 \leq r < s \leq 1$. Then, it follows that

$$E_{r,s} = \mathbb{E}_{z_s} \|(r-s)(u(z_s, r, s) - \hat{u}(z_s, r, s))\|^2, \quad (33)$$

and the right hand side of (31) is simply $E_{0,1}$. Next, we can compute that for any $0 \leq r < s \leq 1$,

$$\begin{aligned}
\frac{\partial}{\partial s} E_{r,s} &= 2\mathbb{E}_{z_s} \left\langle (r-s)(u(z_s, r, s) - \hat{u}(z_s, r, s)), \frac{d}{ds}(r-s)u(z_s, r, s) - \frac{d}{ds}(r-s)\hat{u}(z_s, r, s) \right\rangle \\
&= 2\mathbb{E}_{z_s} \langle (r-s)(u(z_s, r, s) - \hat{u}(z_s, r, s)), -u(z_s, r, s) + \hat{u}(z_s, r, s) \rangle \\
&\quad + 2\mathbb{E}_{z_s} \left\langle (r-s)(u(z_s, r, s) - \hat{u}(z_s, r, s)), (r-s)\frac{du(z_s, r, s)}{ds} - (r-s)\frac{d\hat{u}(z_s, r, s)}{ds} \right\rangle \\
&= 2\mathbb{E}_{z_s} \langle (r-s)(u(z_s, r, s) - \hat{u}(z_s, r, s)), -u(z_s, r, s) + \hat{u}(z_s, r, s) \rangle \\
&\quad + 2\mathbb{E}_{z_s} \left\langle (r-s)(u(z_s, r, s) - \hat{u}(z_s, r, s)), u(z_s, r, s) - v_s(z_s) - (r-s)\frac{d}{ds}\hat{u}(z_s, r, s) \right\rangle \\
&= 2\mathbb{E}_{z_s} \left\langle (r-s)(u(z_s, r, s) - \hat{u}(z_s, r, s)), \hat{u}(z_s, r, s) - v_s(z_s) - (r-s)\frac{d}{ds}\hat{u}(z_s, r, s) \right\rangle \\
&\leq \mathbb{E}_{z_s} \|(r-s)(u(z_s, r, s) - \hat{u}(z_s, r, s))\|^2 \\
&\quad + \mathbb{E}_{z_s} \left\| \hat{u}(z_s, r, s) - v_s(z_s) - (r-s)\frac{d}{ds}\hat{u}(z_s, r, s) \right\|^2 \\
&= E_{r,s} + \mathbb{E}_{z_s} \left\| \hat{u}(z_s, r, s) - v_s(z_s) - (r-s)\frac{d}{ds}\hat{u}(z_s, r, s) \right\|^2 \\
&= E_{r,s} + \varepsilon_{r,s}. \tag{34}
\end{aligned}$$

By product rule and (34), we have

$$\frac{\partial}{\partial s} (e^{-s} E_{r,s}) = -e^{-s} E_{r,s} + e^{-s} \frac{\partial}{\partial s} E_{r,s} \leq e^{-s} \varepsilon_{r,s}. \tag{35}$$

By letting $r = 0$ and integrating s from 0 to 1 in (35), we get

$$e^{-1} E_{0,1} - e^{-1} E_{0,0} = e^{-1} E_{0,1} \leq \int_0^1 e^{-s} \varepsilon_{0,s} ds \leq \int_0^1 \varepsilon_{0,s} ds = \mathbb{E}_s[\varepsilon_{0,s}] \leq \varepsilon, \tag{36}$$

where we used the fact that $E_{0,0} = 0$, which implies that

$$E_{0,1} \leq e\varepsilon. \tag{37}$$

This completes the proof. \square

A.4 Proof of Corollary 1

Proof. Let $x_0 = z_0 = z_1 - u(z_1, 0, 1, x_t, t)$ and $\hat{x}_0 = \hat{z}_0 = z_1 - \hat{u}(z_1, 0, 1, x_t, t)$ where $z_1 \sim \rho_1$. Then $x_0 \sim p_{0|t}$ and $\hat{x}_0 \sim \hat{p}_{0|t}$.

First, given a conditional Mean Flow model $\hat{u} = \hat{u}(z_s, r, s, x_t, t)$, recall that

$$\gamma(r, s, t, x_t) = \mathbb{E}_{z_s} \left[\left\| \hat{u} - \left(v_s(z_s | x_t, t) - (s-r)\frac{d}{ds}\hat{u} \right) \right\|^2 \right]. \tag{38}$$

Under our assumption, $\mathbb{E}_{s,t,x_t}[\gamma(0, s, t, x_t)] \leq \varepsilon < \infty$, which implies that $\mathbb{E}_s[\gamma(0, s, t, x_t)]$ is finite for a.e. t, x_t . Using Theorem 1, we obtain for a.e. t, x_t ,

$$\mathcal{W}_2^2(p_{0|t}, \hat{p}_{0|t}) \leq e\mathbb{E}_s[\gamma(0, s, t, x_t)]. \tag{39}$$

By taking the expectation on both sides, we obtain

$$\mathbb{E}_{t,x_t} [\mathcal{W}_2^2(p_{0|t}, \hat{p}_{0|t})] \leq e\varepsilon, \tag{40}$$

which concludes the proof. \square

A.5 Proof of Proposition 3

Proof. Consider the coupling

$$x_1 = \alpha_1 x_0 + \sigma_1 \epsilon \sim p_1, \quad (41)$$

$$\tilde{x}_1 = \epsilon \sim \tilde{p}_1 = \mathcal{N}(0, I_d), \quad (42)$$

where ϵ is independent of x_0 , $\alpha_1^2 = \exp\left(-\int_0^1 \beta_\tau d\tau\right)$ and $\sigma_1 = \sqrt{1 - \alpha_1^2}$. Given a candidate conditional one-step Mean Flow model \hat{u} , define

$$\hat{x}_0 = z_1 - \hat{u}(z_1, 0, 1, x_1, 1), \quad z_1 \sim \mathcal{N}(0, I_d), \quad x_1 \sim p_1, \quad (43)$$

$$\tilde{x}_0 = z_1 - \hat{u}(z_1, 0, 1, \tilde{x}_1, 1), \quad z_1 \sim \mathcal{N}(0, I_d), \quad \tilde{x}_1 \sim \tilde{p}_1, \quad (44)$$

where z_1 is independent of ϵ , x_0 , x_1 , \tilde{x}_1 , and let \hat{p}_0, \tilde{p}_0 denote distributions for \hat{x}_0, \tilde{x}_0 respectively. Furthermore, under our assumption, the map $\hat{u}(z_1, 0, 1, x_1, 1)$ is L -Lipschitz in x_1 in expectation over z_1 , that is, for any x_1, x'_1 ,

$$\mathbb{E}_{z_1} \left[\left\| \hat{u}(z_1, 0, 1, x_1, 1) - \hat{u}(z_1, 0, 1, x'_1, 1) \right\|^2 \right] \leq L^2 \|x_1 - x'_1\|^2. \quad (45)$$

By the definition of the 2-Wasserstein distance, we obtain

$$\begin{aligned} \mathcal{W}_2^2(\hat{p}_0, \tilde{p}_0) &\leq \mathbb{E} \|\hat{x}_0 - \tilde{x}_0\|^2 \\ &\leq \mathbb{E} \|\hat{u}(z_1, 0, 1, x_1, 1) - \tilde{u}(z_1, 0, 1, \tilde{x}_1, 1)\|^2 \\ &\leq L^2 \mathbb{E} \|x_1 - \tilde{x}_1\|^2 \end{aligned} \quad (46)$$

$$\begin{aligned} &= L^2 \mathbb{E} \|\alpha_1 x_0 + (1 - \sigma_1)\epsilon\|^2 \\ &= L^2 (\alpha_1^2 \mathbb{E} \|x_0\|^2 + (1 - \sigma_1)^2 d) \end{aligned} \quad (47)$$

$$\leq L^2 (\alpha_1^2 m_2 + (1 - \sigma_1)^2 d), \quad (48)$$

where in (46) we used the Lipschitz-in- x_1 property of the flow map, and (47) used the independence of $\epsilon \sim \mathcal{N}(0, I_d)$ and x_0 and the finiteness of $m_2 = \mathbb{E} \|x_0\|^2$.

Hence, we conclude from (48) that

$$\mathcal{W}_2^2(\hat{p}_0, \tilde{p}_0) \leq L^2 (\alpha_1^2 m_2 + (1 - \sigma_1)^2 d). \quad (49)$$

This completes the proof. \square

A.6 Proof of Corollary 2

By applying the triangle inequality for the 2-Wasserstein distance, Young's inequality and Proposition 3, we have

$$\begin{aligned} \mathcal{W}_2^2(\tilde{p}_0, p_0) &\leq 2 (\mathcal{W}_2^2(\tilde{p}_0, \hat{p}_0) + \mathcal{W}_2^2(\hat{p}_0, p_0)) \\ &= 2 (L^2 (\alpha_1^2 m_2 + (1 - \sigma_1)^2 d) + \mathcal{W}_2^2(\hat{p}_0, p_0)). \end{aligned} \quad (50)$$

Since, by assumption, $\mathbb{E}_{s, x_1} [\gamma(0, s, 1, x_1)] \leq \varepsilon_1$, we obtain

$$\begin{aligned} \mathcal{W}_2^2(\hat{p}_0, p_0) &= \mathcal{W}_2^2(\mathbb{E}_{x_1} [\hat{p}_{0|1}(x_0|x_1)], \mathbb{E}_{x_1} [p_{0|1}(x_0|x_1)]) \\ &\leq \mathbb{E}_{x_1} \left[\mathcal{W}_2^2(\hat{p}_{0|1}(x_0|x_1), p_{0|1}(x_0|x_1)) \right] \\ &\leq \mathbb{E}_{s, x_1} [e\gamma(0, s, 1, x_1)] \\ &\leq e\varepsilon_1, \end{aligned} \quad (51)$$

where we applied (39).

Combining Equations (50) and (51), we obtain

$$\mathcal{W}_2^2(\tilde{p}_0, p_0) \leq 2 (L^2 (\alpha_1^2 m_2 + (1 - \sigma_1)^2 d) + e\varepsilon_1), \quad (52)$$

which concludes the proof.

B Additional Technical Results

Proposition 3 relies on a Lipschitz assumption (29). We will show that if we assume \tilde{p}_1 and \hat{p}_1 have bounded support, which naturally arises in the setting when the data distribution p_0 has bounded support, then we can remove this Lipschitz assumption.

Proposition 4. *Let $\hat{p}(x_0|x_t)$ be a candidate conditional Mean Flow model that parametrizes the transition dynamics of the reverse SDE kernel (16), and let $\tilde{p}_1 = \int_{\mathbb{R}^d} \hat{p}(x_0|x_1)\mathcal{N}(x_1; 0, I_d)dx_1$ and $\hat{p}_1 = \int_{\mathbb{R}^d} \hat{p}(x_0|x_1)p(x_1)dx_1$ where $p_1(x_1)$ is the density of x_1 associated with (16). Assuming that \tilde{p}_1 and \hat{p}_1 have bounded support, which is contained in a Euclidean ball centered at the origin with radius $R > 0$ in \mathbb{R}^d , we obtain*

$$\mathcal{W}_2^2(\hat{p}_1, \tilde{p}_1) \leq 2\sqrt{2D_{\text{KL}}(p_0\|\mathcal{N}(0, I_d))}R^2\alpha_1, \quad (53)$$

where α_1 is defined through (15).

Proof. Under our assumption, \tilde{p}_1 and \hat{p}_1 have bounded support, which is contained in a Euclidean ball centered at the origin with radius $R > 0$ in \mathbb{R}^d . Then, the 2-Wasserstein distance can be upper bounded by the total variation (TV) distance (Gibbs & Su, 2002):

$$\mathcal{W}_2(\hat{p}_1, \tilde{p}_1) \leq 2R\sqrt{\text{TV}(\hat{p}_1, \tilde{p}_1)}. \quad (54)$$

Next, we recall that

$$\tilde{p}_1 = \int_{\mathbb{R}^d} \hat{p}(x_0|x_1)\mathcal{N}(x_1; 0, I_d)dx_1, \quad (55)$$

$$\hat{p}_1 = \int_{\mathbb{R}^d} \hat{p}(x_0|x_1)p(x_1)dx_1, \quad (56)$$

where $p_1(x_1)$ is the density of x_1 associated with (16).

By data processing inequality, we get

$$\text{TV}(\hat{p}_1, \tilde{p}_1) \leq \text{TV}(\mathcal{N}(x_1; 0, I_d), p(x_1)). \quad (57)$$

Moreover, by Pinsker's inequality, the TV distance can be upper bounded using the KL divergence as follows:

$$\text{TV}(\mathcal{N}(x_1; 0, I_d), p(x_1)) \leq \sqrt{\frac{1}{2}D_{\text{KL}}(p(x_1)\|\mathcal{N}(x_1; 0, I_d))}. \quad (58)$$

Note that $p(x_1)$ denotes the distribution of x_1 , where x_t follows the Ornstein-Uhlenbeck process (14):

$$dx_t = -\frac{1}{2}\beta_t x_t dt + \sqrt{\beta_t} dw_t, \quad x_0 \sim p_0. \quad (59)$$

By a deterministic time change, one can see that $x_t = y_{\tau(t)}$ in distribution, where y_t follows the rescaled Ornstein-Uhlenbeck process:

$$dy_t = -y_t dt + \sqrt{2} dw_t, \quad y_0 \sim p_0, \quad (60)$$

with

$$\tau(t) := \frac{1}{2} \int_0^t \beta_\tau d\tau. \quad (61)$$

It follows from the proof of Theorem 2 in Chen et al. (2023b) and Theorem 5.2.1. in Bakry et al. (2014) that

$$D_{\text{KL}}(\text{Law}(y_t)\|\mathcal{N}(0, I_d)) \leq e^{-2t}D_{\text{KL}}(\text{Law}(y_0)\|\mathcal{N}(0, I_d)) = e^{-2t}D_{\text{KL}}(p_0\|\mathcal{N}(0, I_d)). \quad (62)$$

Therefore, we have

$$D_{\text{KL}}(\text{Law}(x_t)\|\mathcal{N}(0, I_d)) \leq e^{-2\tau(t)}D_{\text{KL}}(p_0\|\mathcal{N}(0, I_d)). \quad (63)$$

In particular, by letting $t = 1$ with $x_1 \sim p_1$, we obtain

$$D_{\text{KL}}(p_1\|\mathcal{N}(0, I_d)) \leq e^{-2\tau(1)}D_{\text{KL}}(p_0\|\mathcal{N}(0, I_d)) = \alpha_1^2 D_{\text{KL}}(p_0\|\mathcal{N}(0, I_d)), \quad (64)$$

where α_1 is defined through (15).

Hence, by combining (54), (57), (58) and (64), we conclude that

$$\mathcal{W}_2^2(\hat{p}_1, \tilde{p}_1) \leq 2\sqrt{2}R^2\alpha_1 (D_{\text{KL}}(p_0\|\mathcal{N}(0, I_d)))^{1/2}. \quad (65)$$

This completes the proof. \square

By applying Corollary 1 and Proposition 4, we obtain the following corollary which is an analogue of Corollary 2.

Corollary 3. *Under the assumptions of Theorem 1, Corollary 1, and Proposition 4, we have*

$$\mathcal{W}_2^2(\tilde{p}_0, p_0) \leq 2 \left(2\sqrt{2\kappa_0}R^2\alpha_1 + e\varepsilon_1 \right), \quad (66)$$

provided that $\mathbb{E}_{s,x_1}[\gamma(0, s, 1, x_1)] \leq \varepsilon_1$, where $\kappa_0 := \text{D}_{\text{KL}}(p_0 \|\mathcal{N}(0, I_d))$ and α_1 is defined through (15).

Proof. By applying the triangle inequality for the 2-Wasserstein distance, Young's inequality and Proposition 4, we have

$$\begin{aligned} \mathcal{W}_2^2(\tilde{p}_0, p_0) &\leq 2 \left(\mathcal{W}_2^2(\tilde{p}_0, \hat{p}_0) + \mathcal{W}_2^2(\hat{p}_0, p_0) \right) \\ &= 2 \left(2\sqrt{2\text{D}_{\text{KL}}(p_0 \|\mathcal{N}(0, I_d))}R^2\alpha_1 + \mathcal{W}_2^2(\hat{p}_0, p_0) \right). \end{aligned} \quad (67)$$

The rest of the proof follows the same lines as in the proof of Corollary 2 and is hence omitted here. \square

Note that in Corollary 3, the right hand side of (66) can be made small if $\alpha_1 = \exp(-\frac{1}{2} \int_0^1 \beta_\tau d\tau)$ is chosen to be small. Indeed, we have the following corollary.

Corollary 4. *Under the setting of Corollary 3,*

$$\mathcal{W}_2^2(\tilde{p}_0, p_0) \leq 2 \left(2\sqrt{2}R^2 + e \right) \varepsilon_1, \quad (68)$$

provided that $\alpha_1 \leq \varepsilon_1 / \sqrt{\kappa_0}$.

Proof. It is an immediate consequence of Corollary 3. \square

Similarly, for Corollary 2 for the distributions with unbounded support, the right hand side of (30) in Corollary 2 can be made small if $\alpha_1 = \exp(-\frac{1}{2} \int_0^1 \beta_\tau d\tau)$ is chosen to be small. Indeed, we have the following corollary.

Corollary 5. *Under the setting of Corollary 2,*

$$\mathcal{W}_2^2(\tilde{p}_0, p_0) \leq 2 \left(L^2 + e \right) \varepsilon_1, \quad (69)$$

provided that $\alpha_1 \leq \sqrt{\frac{-m_2 + \sqrt{m_2^2 + 4\varepsilon_1 d}}{2d}}$.

Proof. First, we recall from Corollary 2 that

$$\mathcal{W}_2^2(\tilde{p}_0, p_0) \leq 2 \left(L^2 \left(\alpha_1^2 m_2 + (1 - \sigma_1)^2 d \right) + e\varepsilon_1 \right), \quad (70)$$

where $\alpha_1 = \exp(-\frac{1}{2} \int_0^1 \beta_\tau d\tau)$ and $\sigma_1 = \sqrt{1 - \alpha_1^2}$.

Next, we can compute that

$$\begin{aligned} \alpha_1^2 m_2 + (1 - \sigma_1)^2 d &= \alpha_1^2 m_2 + \left(1 - \sqrt{1 - \alpha_1^2} \right)^2 d \\ &= \alpha_1^2 m_2 + \left(\frac{\alpha_1^2}{1 + \sqrt{1 - \alpha_1^2}} \right)^2 d \\ &\leq \alpha_1^2 m_2 + \alpha_1^4 d \leq \varepsilon_1, \end{aligned} \quad (71)$$

provided that $\alpha_1^2 \leq \frac{-m_2 + \sqrt{m_2^2 + 4\varepsilon_1 d}}{2d}$. This completes the proof. \square

C Inverse Problems Using STMD

Inverse problems aim at constructing samples from the high dimensional distributions given partial observations. For example, in the context of Section 3.1, consider the problem of generating samples from the data distribution $x_0 \sim p_0$, conditional on noisy observations

$$y = \mathcal{A}(x_0) + \eta, \quad \eta \sim \mathcal{N}(0, \sigma_y^2 I_n), \quad (72)$$

where \mathcal{A} is a linear or nonlinear measurement operator and $y \in \mathbb{R}^n$ with $n < d$. There are many methods in the literature for solving such problems; see, for example, Song et al. (2021); Chung et al. (2023); Graikos et al. (2025); Peng et al. (2025) and the references therein. Because solving inverse problems is not the primary purpose of our work, we will follow the simple setup of Wang et al. (2023), and leave the design of an inverse problem solver tailored to our STMD algorithm for future work. To this end, given linear and noiseless measurement $y = Mx$, where $M \in \mathbb{R}^{n \times d}$, and using $M^+ = M^\top(MM^\top)^{-1}$, we provide the following simple inference algorithm.

Algorithm 3 STMD conditional inference

Input: Trained model $u^\theta(z_s, r, s, x_t, t)$, initial samples $x_1 \sim \mathcal{N}(0, I_d)$, number of inference steps n_{inf} , number of Mean Flow steps n_{mf} , mask M , observation $y = Mx_0$.

```

 $\Delta t \leftarrow \frac{1}{n_{\text{inf}}}, \Delta s \leftarrow \frac{1}{n_{\text{mf}}}, t \leftarrow 1$ 
for  $k$  in  $\text{range}(n_{\text{inf}})$  do:
     $z_1 \sim \mathcal{N}(0, I_d), s \leftarrow 1$ 
    for  $i$  in  $\text{range}(n_{\text{mf}})$  do:
         $z_{s-\Delta s} \leftarrow z_s - \Delta s u^\theta(z_s, s - \Delta s, x_t, t)$ 
         $s \leftarrow s - \Delta s$ 
    end for
     $x_0 \leftarrow z_0$ 
     $x_0 \leftarrow M^+ y + (1 - M^+ M) x_0$ 
     $x_{t-\Delta t} \sim p(x_{t-\Delta t} | \bar{x}_0, x_t)$  from Equation (19)
     $x_t \leftarrow x_{t-\Delta t}$ 
     $t \leftarrow t - \Delta t$ 
end for
return  $x_0$ 

```

D Experimental Details

The MNIST and CIFAR10 experiments use U-Net architectures using the diffusers library. We list some key parameters of the networks below in Table 1.

Table 1: Network parameters for MNIST and CIFAR10.

Feature	MNIST	CIFAR10
Total Params	1.1 M	37.5 M
Down Block Types	{DownBlock2D, AttnDownBlock2D, DownBlock2D}	{DownBlock2D, AttnDownBlock2D, DownBlock2D, DownBlock2D}
Up Block Types	{UpBlock2D, AttnUpBlock2D, UpBlock2D}	{UpBlock2D, UpBlock2D, AttnUpBlock2D, UpBlock2D}
Block Out Channels	{32, 64, 32}	{128, 256, 256, 256}
Layers per Block	1	2
Time Embedding Type	positional	positional
Activation Function	SiLu	SiLu
Downsample Padding	1	0
Input Sample Size	1x28x28	3x32x32

We train with the following parameters in each experiment summarized in Table 2.

Table 2: Training hyperparameters for MNIST and CIFAR10.

Hyperparameter	MNIST	CIFAR10
Learning rate	0.0005	0.0001
Total number of iterations	150K	450K
Batch size	64	64
EMA decay	.9995	.9995

Furthermore, following Geng et al. (2025a,b), for each loss function $\mathcal{L} = \|\Delta\|^2$ (where Δ is, for example, the term inside the form of (13)), we train using the adaptive loss $\text{sg}(w) \cdot \mathcal{L}$ where

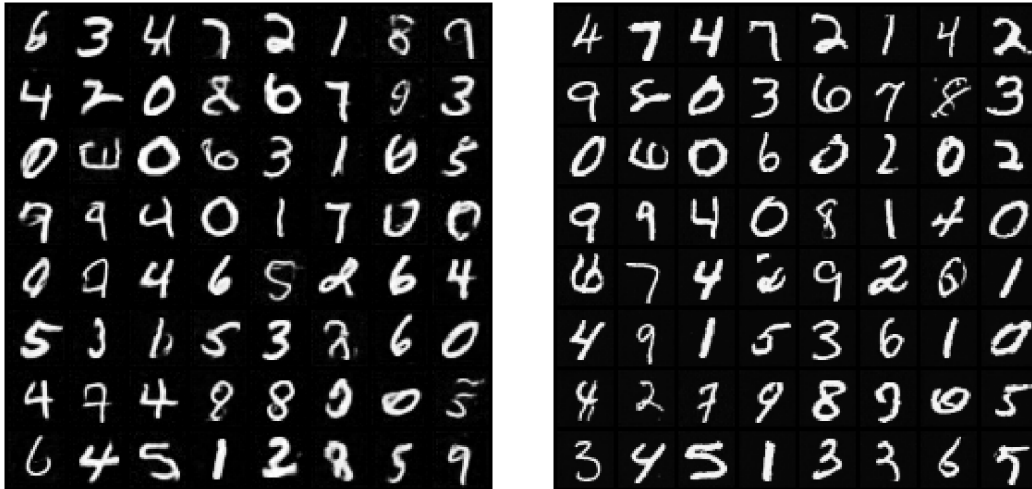
$$w = \frac{1}{(\|\Delta\|^2 + c)^p}, \quad (73)$$

for $c = 0.01$ and $p = 1$. We use a lognorm sampler for r, s with ratio 75% $r \neq t$. We refer to Geng et al. (2025a) and their public code repository for further details.

Regarding the benchmark metric calculation for the MNIST experiment, as using the features of the InceptionV3 network is unreliable (Song & Ermon, 2019), we trained a custom classifier and used its final-layer latent features for calculating the Fréchet distance. Our evaluation model is a lightweight convolutional neural network consisting of two convolutional layers followed by two fully connected layers. To calculate the FD, we extract the 128-dimensional pre-ReLU activations from the penultimate layer, providing a more stable representation.

For the CelebA example, we use a custom DiT model from the public Mean Flow repository ¹, with `depth=16`, `hidden_size=1024`, `patch_size=2`, `num_heads=16`, and a total number of 308M trainable parameters. We use the pretrained autoencoder from Stable Diffusion². We train for 400K iterations with a batch size of 16 and a step size of 0.0001. Finally, we provide additional generated images for all of our experiments.

D.1 Additional MNIST Images



(a) $n_{\text{inf}} = 1, n_{\text{mf}} = 1$

(b) $n_{\text{inf}} = 2, n_{\text{mf}} = 2$

Figure 7: MNIST generation results.

¹<https://github.com/Gsunshine/meanflow>

²<https://huggingface.co/stabilityai/sd-vae-ft-ema>

D.2 Additional CIFAR10 Images



(a) $n_{\text{inf}} = 1, n_{\text{mf}} = 1$

(b) $n_{\text{inf}} = 4, n_{\text{mf}} = 2$

Figure 8: CIFAR10 generation results.

D.3 Additional CelebA images



Figure 9: CelebA generation with $n_{\text{inf}} = 4, n_{\text{mf}} = 2$